Journal of Power Sources 242 (2013) 844–847

Contents lists available at SciVerse ScienceDirect

Journal of Power Sources

journal homepage: www.elsevier.com/locate/jpowsour

Short communication

Analysis of hard carbon for lithium-ion batteries by hard X-ray photoelectron spectroscopy

Hironobu Hori [a,1], Masahiro Shikano [a,*], Hironori Kobayashi [a], Shinji Koike [a], Hikari Sakaebe [a], Yoshiyasu Saito [b], Kuniaki Tatsumi [a], Hideki Yoshikawa [c], Eiji Ikenaga [d]

[a] Research Institute for Ubiquitous Energy Devices, AIST, 1-8-31 Midorigaoka, Ikeda, Osaka 563-8577, Japan
[b] Energy Technology Research Institute, AIST, AIST Tsukuba Central 2, 1-1-1 Umezono, Tsukuba, Ibaraki 305-8568, Japan
[c] Beamline Station, National Institute for Materials Science (NIMS), 1-1-1 Kouto, Sayo-cho, Sayo-gun, Hyogo 679-5148, Japan
[d] Japan Synchrotron Radiation Research Institute (JASRI), 1-1-1 Kouto, Sayo-cho, Sayo-gun, Hyogo 679-5198, Japan

HIGHLIGHTS

- Lithium insertion mechanism into hard carbon is discussed.
- ^{7}Li NMR, X-ray photoelectron spectroscopy, and hard X-ray photoelectron spectroscopy are used in this study.
- The existence of different Li insertion sites is proved by these spectra.

ARTICLE INFO

Article history:
Received 5 April 2013
Received in revised form
27 May 2013
Accepted 29 May 2013
Available online 10 June 2013

Keywords:
Lithium-ion battery
Hard carbon
Lithium insertion
X-ray photoelectron spectroscopy
Hard X-ray photoelectron spectroscopy
Nuclear magnetic resonance

ABSTRACT

Non-graphitizable carbon (hard carbon) as a negative electrode material for lithium-ion batteries is investigated by X-ray photoelectron spectroscopy, and hard X-ray photoelectron spectroscopy (HX-PES). HX-PES spectra have peaks of both the solid electrolyte interphase on the hard carbon surface and the hard carbon itself. The change in spectrum with state of charge is observed by HX-PES. Hard carbon has two types of lithium insertion site; between graphene sheets and into nano-scale voids. These spectroscopic results are consistent with the lithium insertion mechanism into hard carbon.

1. Introduction

Lithium-ion batteries, which consist of a nonaqueous electrolyte with carbon as a negative electrode and transition metal oxides containing lithium ion as a positive electrode have been commercialized as power sources for portable electronic equipment, *e.g.*, laptop computers, cellular phones and so on. Despite their associated high energy density, lithium metal electrodes have been plagued with a dendrite growth problem that can result in thermal runaway, and thus carbon materials have come into practical use as negative electrodes [1]. Among the carbonaceous materials studied for use as negative electrodes in lithium-ion batteries, graphite has been widely used in commercial lithium-ion batteries owing to the resulting low working potential, high reversible capacity and other characteristics. Other carbonaceous materials have also been studied in an attempt to enhance the performance of lithium-ion batteries. Hard carbon is a promising candidate material for lithium-ion batteries in hybrid electrical vehicles, offering excellent cyclability and high input/output performances [2].

It is pointed out that the hard carbon should have many pores in the structure because its density is lower than that of graphite. Various structural models for hard carbon have been suggested by Shiraishi [3], Franklin [4] and Jenkins *et al.* [5]. Based on these models, representative lithium intercalation mechanisms of the

* Corresponding author. Tel.: +81 72 751 7932.
E-mail address: shikano.masahiro@aist.go.jp (M. Shikano).
[1] Present address: Institute for Materials Chemistry and Engineering, Kyushu University, 6-1 Kasuga-Koen, Kasuga-city, Fukuoka 816-8580, Japan.

0378-7753/$ – see front matter © 2013 Elsevier B.V. All rights reserved.
http://dx.doi.org/10.1016/j.jpowsour.2013.05.160

hard carbon are known as the card-house model [6] and the wave model [7]. Although results of X-ray diffraction and transmission electron microscopic observations suggest that these structural models have a low crystalline and complex internal structure, their details and sites of lithium have remained unclear. Recently, Nagao *et al.* [8] reported their results of crystal structural analyses for hard carbon using X-ray and neutron diffraction-pattern simulation, neutron small-angle scattering and neutron total scattering techniques, showing that the state of lithium in hard carbon is very similar to the wave model. In the case of $E < 0.1$ V *vs.* Li/Li^+, lithium occupies the nano-void formed by stacking faults in two-dimensional graphene layers, and a large capacity occurs. Lithium in hard carbon has at least two states: between graphene sheets, like graphite, and in nano-voids. The states of lithium in hard carbon have been characterized by ^7Li nuclear magnetic resonance (NMR) which reveals two kinds of lithium; ionic and metallic [9,10]. X-ray photoelectron spectroscopy (XPS) is a common tool to investigate the electronic state of elements in compounds. Electrochemically lithiated carbon has a solid electrolyte interphase (SEI) on the surface, which behaves a barrier to the XPS measurement. Although XPS using argon sputtering can be used to determine the depth profile of the SEI, the details of lithium in carbon materials have not been thoroughly evaluated.

The hard X-ray photoelectron spectroscopy (HX-PES) is a powerful tool to observe active materials directly under the SEI and/or the sediment because its probe depth is several tens of nanometers and insensitive to the surface condition. In the case of the positive electrode, decomposition products of the electrolyte also amass on the surface of electrodes [11,12]. These sediments are very thin but present a barrier to XPS measurement, like the SEI of the negative electrode. Argon sputtering is not suitable in case of the positive electrode because the whole product on the surface is blown away and active material is reduced very easily. We have already successfully observed its surface directly by HX-PES in a synchrotron facility [12] and clarified the superiority of HX-PES for the surface analysis of electrode. In this study, we report our direct observation of a negative electrode behind the SEI by HX-PES, and the lithium condition of hard carbon is discussed. ^7Li NMR measurements are also carried out for comparison.

2. Experimental

We used 18650-type cylindrical cells of capacity *ca.* 380 mA h for this study. These were designed to have a rate capability of more than 10 C. The cells were constructed from pressed double-side coated electrodes using a high-power design; the positive electrode was comprised of $LiNi_{0.80}Co_{0.15}Al_{0.05}O_2$ (NCA, Toda Kogyo Corp.), acetylene black (AB, DENKA) and poly(vinylidene difluoride) (PVDF, Kureha Corp.) binder, and the negative electrode consisted of non-graphitizable carbon (hard carbon, Kureha Corp.) and PVDF (Kureha Corp.) binder. 1 mol dm^{-3} $LiPF_6$ in ethylene carbonate (EC)/dimethyl carbonate (DMC) with a volume ratio of 1:2 was used as the electrolyte.

The state of charge (SOC) for cells was controlled from 0% to 90% and disassembled in a glove box under dry argon. The electrodes were soaked for more than 2 min in DMC to remove remnant $LiPF_6$, and then used as samples after drying *in vacuo* at room temperature for more than 10 h. A pristine electrode, never exposed to electrolyte, was prepared as a reference sample.

HX-PES was performed at BL47XU/SPring-8 with the approval of the JASRI. The X-ray photon energy was *ca.* 6.0 keV. The total energy resolution was estimated as 240 meV from Fermi edge of Au measurement. The peak position of the C1s with the highest binding energy was assumed to be caused by $-CF_2-$ of PVDF and set to 290.5 eV as a reference point for the sample charge-up correction. The C1s profiles were decomposed into six peaks and Shirley's background by the curve-fitting software XPSPEAKS 4.1. Conventional XPS measurements were also performed on a PHI 5000 VersaProbe (ULVAC-PHI) with monochromatic Al Kα (1.4866 keV). Charging effects by the poor surface conductivity were minimized by applying a 10 eV argon ion gun. In both cases, sealed vessels were used to transfer samples from the glove box to the analyzer chamber in order to avoid air exposure.

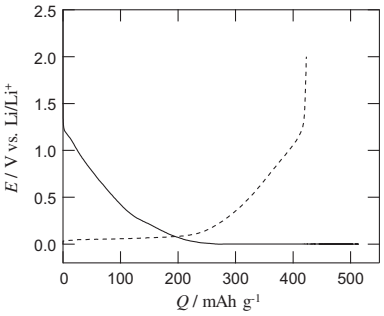

Fig. 1. First galvanostatic charge (lithium insertion process; solid line) and discharge (lithium extraction process; dashed line) curves of a hard carbon/lithium metal cell.

The lithiated hard carbons were examined by ^7Li NMR spectroscopy. The electrodes were put in NMR sample tubes in a dry box and set into a wideline probe of a ^7Li NMR spectrometer ($B_0 = 4.70$ T; ν_0 (^7Li) = 77.8 MHz; CMX-200H, Chemagnetics Corporation). Line shift δ was measured with aqueous LiCl solution as an external standard.

3. Results and discussion

Based on previous studies [8,13,14], lithium occupies sites between graphene layers above 0.1 V *vs.* Li/Li^+ and in nano-scale voids below 0.1 V *vs.* Li/Li^+. Fig. 1 shows an initial charge–discharge curve of a half-cell consisting of lithium metal and hard carbon electrodes. As shown in Fig. 1, a very large capacity is observed below 0.1 V *vs.* Li/Li^+, and irreversible capacity accompanied by the formation of the SEI is observed. From this result, the relationship between the SOC of the 18650-type cylindrical cells and the potential (*vs.* Li/Li^+) of the hard carbon electrode can be evaluated as summarized in Table 1. For example, SOC = 70% means that the negative electrode is almost 0.1 V *vs.* Li/Li^+.

Fig. 2(a) and (b) shows C 1s and Li 1s core-level spectra for hard carbon electrodes, respectively. The pristine sample has two peaks at 284.5 and 290.0 eV in the C 1s spectrum. The former peak relates to graphene layer parts in hard carbon [15,16] and the latter peak is assigned to $-CF_2-$ in PVDF [17,18]. A peak of $-CH_2-$ in PVDF, which can be observed at 286.0 eV [17,18], overlaps with the slope of the former peak. Samples of lithiated hard carbon have two peaks at 284.0 and 289.0 eV, which are almost independent of SOC. These peaks are assigned to the SEI, which consists of hydrocarbon, organic carbonates, lithium carbonate and so on [19–21]. The peak at 55.0 eV in the Li 1s spectrum corresponds to LiF and/or Li_2CO_3 in the SEI. It is very difficult to decompose these peaks because of the

Table 1
Relationship between SOC and negative electrode potential.

SOC/%	Electrode potential/V *vs.* Li/Li^+
0	0.540
30	0.283
50	0.204
70	0.096
90	0.072

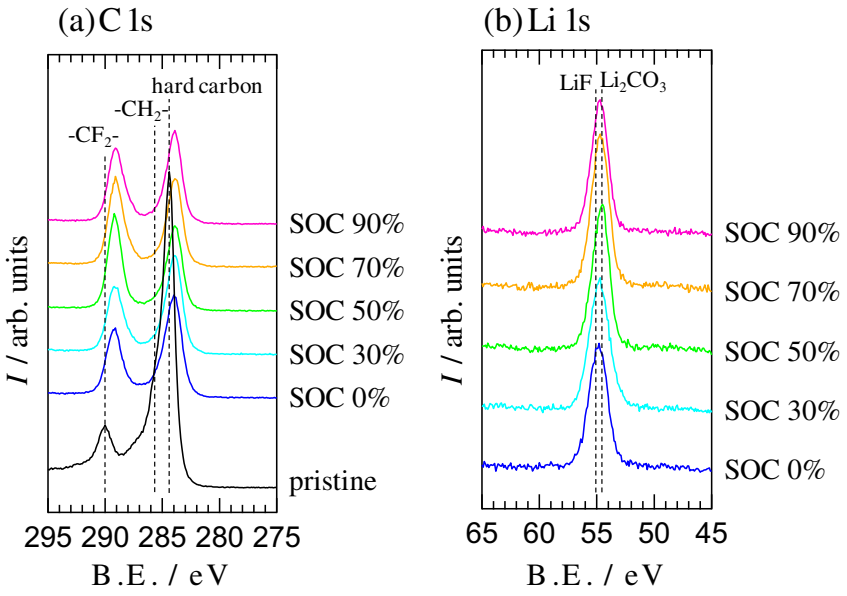

Fig. 2. (a) C 1s and (b) Li 1s core-level XPS spectra of hard carbon electrodes with various SOCs.

small differences between their positions [17]. With HX-PES, the higher excitation energy of 6.0 keV affords greater kinetic energy to the photoelectrons than with conventional XPS. Photoelectrons can escape from a deeper area below the surface, and one can therefore directly observe the spectrum of hard carbon behind the SEI. As shown in Fig. 3(a), the C 1s core-level HX-PES spectra of the hard carbon electrodes with various SOC were significantly different from the conventional XPS spectra (Fig. 2(a)) because the spectra of HX-PES contain both surface and bulk information of the negative electrode, that is, the HX-PES spectra have peaks of not only the SEI but also the hard carbon and the binder of PVDF. Thus, the C 1s core-level HX-PES spectra can be decomposed as shown in Fig. 3(a). The peak at 290.5 eV is due to $-CF_2-$ of PVDF and/or CO_3^{2-} CO_2^{3-} of Li_2CO_3. The peaks at 284.7 and 285.7 eV show $-CH_2-$ of PVDF and/or hydrocarbons and organic carbonates in the SEI. The right peak at around 283.0 eV should relate to hard carbon although its binding energy is lower than that of pristine hard carbon. The binding energy of the C 1s core-level spectrum for lithiated hard carbon may show a peak of lower energy because of its electrical neutrality.

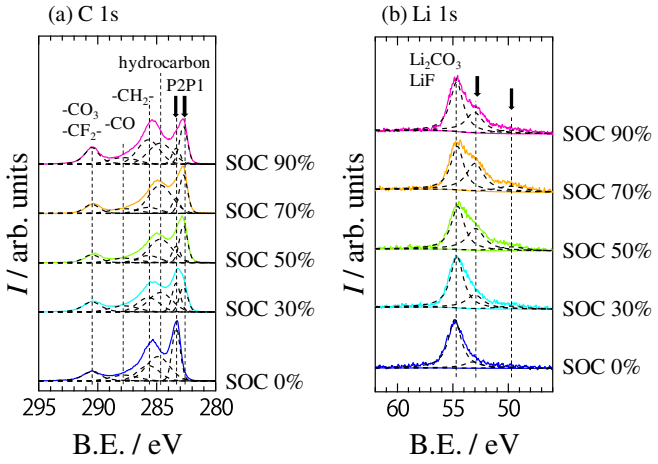

Fig. 3. Peak decomposition in (a) C 1s and (b) Li 1s core-level HX-PES spectra of hard carbon electrodes with various SOCs. Arrows show peaks related to hard carbon itself.

The conventional XPS C1s peak for graphitic carbon with defects could be divided into two parts – one is the graphitic part and the other is the 'defect' part [16]. Peak at around 283.0 eV can be assigned to lithiated hard carbon and decomposed into two components at 282.7 eV (P1) and 283.3 eV (P2) as shown in Fig. 3(a). Fig. 4 shows relative intensity of P1 ($=I_{P1}/(I_{P1}+I_{P2})$) with various SOCs. Relative intensity of P1 increased monotonously at SOC <70% and then was saturated at SOC >70%. Lithium is intercalated between the graphene layers at SOC <70%, while lithium is inserted into the nano-scale voids at SOC >70%. Therefore, P1 should be concerned with carbon near lithium between the graphene layers [22]. Fig. 3(b) shows the Li 1s core-level HX-PES spectra of hard carbon electrodes with various SOC. As mentioned in Fig. 2(b), the peak at 55.0 eV mainly relates to SEI components. For high SOC samples, intensity of a shoulder at around 53.0 eV seems to be saturated. In addition, another broad peak exists at around 51.0 eV. These peaks should be related to the lithium insertion mechanism into the hard carbon and the peaks at around 283.0 eV in C 1s spectra.

Fig. 5 shows ^{7}Li NMR of negative electrodes of various SOCs. The line shift of the resonance peak is unchanged below SOC = 50%, while increases with SOC above 70%. ^{7}Li NMR studies of lithiated hard carbon shows that its line shift depends directly on SOC when lithium occupies nano-voids of hard carbon [10,13,23]. In early

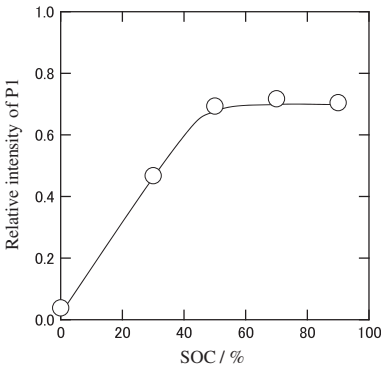

Fig. 4. Relative intensity variation of a peak at 282.7 eV in HX-PES C 1s core-level spectra.

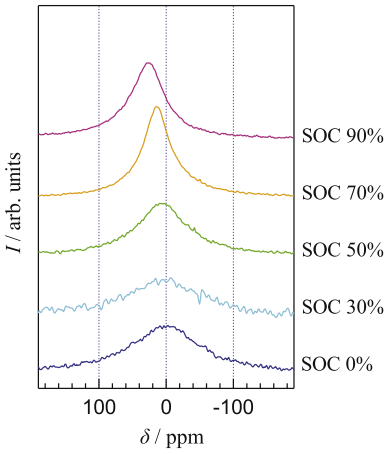

Fig. 5. ^{7}Li NMR spectra of hard carbon electrodes with various SOCs.

charging, lithium should intercalate between graphene sheets, and then the resonance peak maintains same position. The peak intensity at 53.0 eV in the HX-PES spectra of Li 1s core level increases with increasing SOC below 70%. These phenomena are consistent with the results of ^{7}Li NMR studies. Therefore, this peak could be assigned to the lithium between the graphene layers. Studies of ^{7}Li NMR at low temperature showed the signal of lithium in the nano-void sites in hard carbon [9,23,24]. Lithium in the nano-voids exists as clusters of semi-metallic lithium, and the size of the clusters is not uniform because of the distribution of nano-void sizes [23]. Li 1s spectra of HX-PES showed a broad peak at around 50.0 eV in the case of SOC >50%, which could be assigned to the clusters of lithium in the nano-voids. The peak intensity increased above SOC = 50% because lithium in the nano-voids increased.

4. Summary

Analyses of XPS and HX-PES were carried out to investigate the hard carbon negative electrode of the 18650-type cylindrical cell. HX-PES spectra could be assigned by comparison with the XPS results and contained information on both the solid electrolyte interphase (SEI) and the hard carbon. The presence of different Li insertion sites was proven by core-level C 1s and Li 1s spectra. HX-PES is a useful tool to investigate the mechanism of lithium insertion into the negative electrode. We will use them to study the relationship between the lithium insertion mechanism and degradation of negative electrode materials.

Acknowledgments

Part of this work was supported by the “Lithium-ion and Excellent Advanced Batteries Development (Li-EAD) Project” of the New Energy and Industrial Technology Development Organization (NEDO) in Japan. In preliminary experiments, we confirmed the detection of lithium in the hard carbon electrode used in this study by HX-PES in SPring-8/BL15XU. We are grateful to Drs. H. Tanaka and K. Kobayashi of National Institute for Materials Science (NIMS) in Japan for their support in the preliminary experiments.

References

[1] M. Winter, J.O. Besenhard, M.E. Spahr, P. Novák, Adv. Mater. 10 (1998) 725–763.
[2] H. Fujimoto, K. Tokumitsu, A. Mabuchi, N. Chinnasamy, T. Kasuh, J. Power Sources 195 (2010) 7452–7456.
[3] M. Shiraishi, Tanso Zairyou Nyuumon, Kagaku Gijutsu-Sha, Tokyo, 1984, pp. 29–40.
[4] R.E. Franklin, Proc. R. Soc. London, Ser. A 209 (1951) 196–218.
[5] G.M. Jenkins, K. Kawamura, L.L. Ban, Proc. R. Soc. London, Ser. A 327 (1972) 501–517.
[6] T. Zheng, J.S. Xue, J.R. Dahn, Chem. Mater. 8 (1996) 389–393.
[7] J. Conard, P. Lauginie, Tanso 191 (2000) 62–70.
[8] M. Nagao, C. Pitteloud, T. Kamiyama, T. Otomo, K. Itoh, T. Fukunaga, K. Tatsumi, R. Kanno, J. Electrochem. Soc. 153 (2006) A914–A919.
[9] K. Tatsumi, J. Conard, M. Nakahara, S. Menu, P. Lauginie, Y. Sawada, Z. Ogumi, Chem. Commun. (1997) 687–688.
[10] K. Guérin, M. Ménétrier, A. Février-Bouvier, S. Flandrois, B. Simon, P. Biensan, Solid State Ionics 127 (2000) 187–198.
[11] A.M. Andersson, D.P. Abraham, R. Haasch, S. MacLaren, J. Liu, K. Amine, J. Electrochem. Soc. 149 (2002) A1358–A1369.
[12] M. Shikano, H. Kobayashi, S. Koike, H. Sakaebe, E. Ikenaga, K. Kobayashi, K. Tatsumi, J. Power Sources 174 (2007) 795–799.
[13] K. Tatsumi, T. Kawamura, S. Higuchi, T. Hosotubo, H. Nakajima, Y. Sawada, J. Power Sources 68 (1997) 263–266.
[14] P. Novák, D. Goers, M.E. Spahr, in: F. Béguin, E. Frąckowiak (Eds.), Carbons for Electrochemical Energy Storage and Conversion Systems, CRC Press, Boca Raton, 2009, pp. 263–328.
[15] G.K. Wertheim, P.T.Th.M. Van Attekum, S. Basu, Solid State Commun. 33 (1980) 1127–1130.
[16] H. Estrade-Szwarckopf, Carbon 42 (2004) 1713–1721.
[17] J.F. Moulder, W.F. Stickle, P.E. Sobol, K.D. Bomben, in: J. Chastain, R.C. King Jr. (Eds.), Handbook of X-ray Photoelectron Spectroscopy, ULVAC-PHI, Chigasaki, 1995.
[18] M.D. Duca, C.L. Plosceanu, T. Pop, J. Appl. Polym. Sci. 67 (1998) 2125–2129.
[19] K. Kanamura, S. Shiraishi, H. Takezawa, Z. Takehara, Chem. Mater. 9 (1997) 1797–1804.
[20] A.M. Andersson, A. Henningson, H. Siegbahn, U. Jansson, K. Edström, J. Power Sources 119–121 (2003) 522–527.
[21] V. Eshkenazi, E. Peled, L. Burstein, D. Golodnitsky, Solid State Ionics 170 (2004) 83–91.
[22] D. Bar-Tow, E. Peled, L. Burstein, J. Electrochem. Soc. 146 (1999) 824–832.
[23] S.E. Hayes, R.A. Guidotti, W.R. Even Jr., P.J. Hughes, H. Eckert, J. Phys. Chem. A 107 (2003) 3866–3876.
[24] K. Gotoh, M. Maeda, A. Nagai, A. Goto, M. Tansho, K. Hashi, T. Shimizu, H. Ishida, J. Power Sources 162 (2006) 1322–1328.